Texture of Crystalline Solids
1977, Vol. 2, pp. 205-223

THE ORIENTATION AND POSITION ACCURACY OF ELECTRON DIFFRACTION

B. J. DUGGAN and I. P. JONES
Department of Physical Metallurgy and Science of Materials, University of Birmingham, Birmingham, B15 2TT, U.K.

(Received January 25, 1977)

Abstract: The misorientations existing between subgrains are of critical importance in understanding the nucleation and growth of recrystallised grains. In this paper it is demonstrated that, because of spherical aberration and focus error in the objective of a conventional 100 kV electron microscope, the accuracy of beam direction determination is a function of the size of the area selected, when this area is small. Various factors are discussed, and it is shown that for beam direction determination to within 2° accuracy over the whole unit triangle using a modern 100 kV microscope, that the minimum area must be greater than 1.5 μm diameter. The implications of this on previous conventional SAD deformation texture studies, where the subgrain size is typically ∿ 2,500 Å, are discussed.

1. INTRODUCTION

Until quite recently the only convenient way to determine the orientation relationships between small neighbouring volumes of material has been the selected area diffraction technique available in conventional 100 kV electron microscopes. The type of diffraction information obtained depends on the perfection of the crystal; when this is high, inelastic or diffuse scattering may provide very precise orientation information from Kikuchi line analysis. On the other hand, where the crystal concerned is severely dislocated, only spot patterns are available. The general principles of texture determination using electron diffraction have been reviewed.[1] Various ambiguities peculiar to spot patterns have also been discussed.[2,3]

Unfortunately, because of spherical aberration and defocus, each point in the plane of the diffraction pattern

corresponds to a different area of the specimen. This is obviously trivial for large single crystals but when the volume concerned is less than 1 μm diameter then this positional uncertainty becomes limiting. At about the same point it often happens that orientation information has to be derived from spot patterns, as inelastic scattering becomes too weak to be useful.

Two developments which improve the area selection problem have recently occurred: conventional high voltage electron microscopy (HVEM) and scanning transmission electron microscopy (STEM). In a high voltage microscope the diffracting angles are smaller and therefore positional uncertainty is reduced. In STEM the area may be selected at the plane of the specimen by restricting the beam diameter, thus making area selection independent of orientation.

In this paper we first discuss factors affecting orientation data derived from spot patterns, and the positional uncertainty of selected area diffraction. Their interrelationship is considered and finally, previously published results of deformed metal studies are discussed in the light of these findings.

2. ACCURACY OF AREA SELECTION

The conventional method of selected area diffraction is to insert an aperture in the first plane conjugate to the specimen after the objective lens. The aperture can be of any shape; when it is circular it corresponds to an area on the specimen of d/M in diameter, where d is the aperture diameter and M the objective magnification.

Because of the spherical aberration of the objective lens, and defocussing errors, a beam at an angle α to the optic axis of the microscope (assumed here to be the main beam) originates from an area on the specimen which is displaced by an amount ΔR, where

$$\Delta R = C_s \alpha^3 + D\alpha \qquad (1)$$

where C_s = spherical aberration constant of the objective lens.

D = defocus

α = 2 x Bragg angle.

The area selected, when ΔR is small compared with d/M, is of diameter d/M. When ΔR is significant with respect to d/M, however, then the area selected depends upon the detailed geometry of the diffraction pattern, i.e. the area selected becomes a function of the orientation of the foil.

In order to simplify this situation an attempt is made in the following sections to arrive at a minimum value of α, α_{min}, necessary in order to generally determine orientation to within specified limits of accuracy. This value of α_{min} is assumed to define a circle of radius $|g|_{max}$ in the diffraction pattern,and from this it is possible to specify the

area selected as having a diameter L, given by

$$L = \frac{d}{M} + 2(C_s\alpha^3 + d\alpha). \qquad (2)$$

3. ORIENTATION DETERMINATION

It is emphasized that here we are concerned with orientation determination by spot patterns, not by intrinsically inelastic scattering such as Kikuchi lines. The specimen is usually a thin plate, which implies a relaxation of one of the Laue conditions, and therefore the reciprocal lattice points corresponding to the crystal planes are spiked normal to the plate. In the Ewald sphere construction, Figure 1,

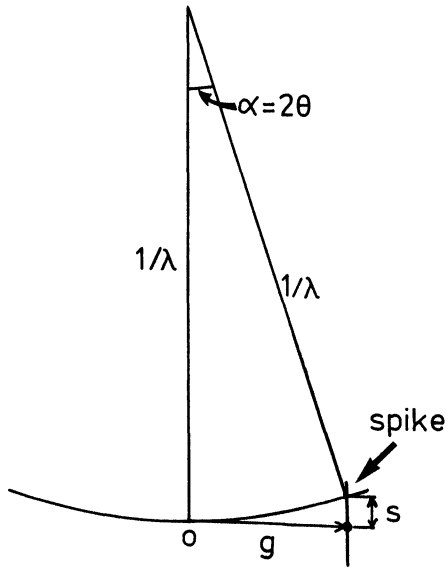

Figure 1. Ewald sphere construction showing the intersection of a sphere of radius $1/\lambda$ with a spiked diffraction spot. The intensity variation along the spike is given by standard kinematical theory.

the intersection of a sphere of radius $1/\lambda$ with this three dimensional array of reciprocal lattice spikes produces the observed diffraction pattern. In general the spike length is inversely proportional to both $|g|$ and to the extinction distance ξ_g, unless the foil is thinner than ξ_g. The variation in intensity along a spike can be adequately described for the vast majority of spots in a diffraction pattern by the kinematical theory. The diffracted intensity for beam g is

$$\exp(-\mu t)\,\frac{\sin^2 \pi t s_g}{w_g^2} \tag{3}$$

where t = crystal thickness.

s_g = deviation of beam g from Ewald sphere.

$w_g = s_g \xi_g$.

μ = mean absorption coefficient of crystal.

This can be further approximated to

$$I \propto \frac{1}{w_g^2} \tag{4}$$

for the case of a parallel sided, flat crystal because of the spread in s_g introduced by beam divergence, inelastic scattering, and foil buckling, and because of small random changes in t.

Unless intensity is taken into account in determining beam directions which are close to low index zones, large errors are likely. Laird, Eichen and Bitler[4] showed that certain small g vector spots can persist over angles of $\sim 30°$ and using the simple cross product of these to determine orientation can therefore be very inaccurate. An obvious improvement is to select the two brightest reflections in the diffraction pattern, as suggested by Ryder and Pitsch.[5] These authors took into account the finite Bragg angles involved and corrected for the fact that different spots are associated with different scattering factors by assuming that intensity was proportional to $|g|^{-4}$. (This depends on the spots being at the Bragg position and the scattering factor, f, inversely proportional to $|g|^2$.) By selecting different pairs of spots they estimated the accuracy of the method to be better than 2°. The same authors introduced a further refinement which is useful when there are three strongly diffracted beams from two different zones.[6] The beams are all assumed to lie on the Ewald sphere and a simple vector formula which is independent of the camera length is employed. The accuracy of this method is better than 1°. We have found these methods to be satisfactory when the basic assumptions are substantially true. They fail, however, in some parts of orientation space where only one systematic row is strongly excited, and then it is necessary to use a slightly more sophisticated approach which is described in Section 4, together with an example.

It is necessary now to consider factors which affect intensity in a diffraction pattern as it is clear that in any specified set of circumstances there will be a minimum spot intensity which we must accept in order to determine beam directions satisfactorily. This will correspond to a particular value of w. This limit is not necessarily one of

intensity, but may be one of diffuseness which makes it difficult to compare the spot's intensity with that of other sharper spots (and probably invalidates Equation 4 in any case). The limit will also vary considerably with foil thickness and absorption coefficient μ. Keeping these reservations in mind, however, it is useful to consider the relationship between w_{max} and parameters important to both orientation determination and area selection by aperture.

Size of g vector

The sampling of the reciprocal lattice is improved, and the probability of finding diffraction spots excited above the minimum brightness necessary for orientation analyses increases, as $|g|_{max}$ is raised. Using copper as an example we have calculated the variation of w_{max} with $|g|_{max}$, where w_{max} corresponds to the weakest diffracted beam that must be used in order that any beam direction in the standard triangle may be analysed. w_{max} was calculated by examining a large number of beam directions distributed uniformly throughout the standard triangle. A beam direction was considered to be identifiable if two non-systematic reflections were visible. For each beam direction in turn, w was evaluated for all possible reflections within g_{max}, and the two lowest values of w for non-systematic reflections (i.e. the two brightest beams, from Equation 4) were stored. w_{max} was the maximum of all these stored values of w. The angular spacing between the beam directions was reduced, and the calculation repeated, until w_{max} converged, which it generally did at $\sim 1/2°$. By performing the calculation in this way, we ignore any possible limitation to w_{max} due to spot diffuseness as previously discussed. This is not expected to have any profound effect upon the form of the results. These are shown in Figure 2.

If the reciprocal lattice points were of identical spike length and randomly distributed in reciprocal space, and similar conditions applied for orientation analyses (i.e. at least two spikes intersecting the Ewald sphere) then $w_{max} \propto \frac{1}{|g|^2}$. It is clear that the actual values of w_{max} depend far less strongly on $|g|$. Three reasons may be advanced for this.

(i) The real lattice is discrete.
(ii) Pairs of systematic reflections do not yield any extra information.
(iii) Extinction distances increase with $|g|$.

In Figure 2 there is also a curve for w_{max}, where ξ_g (i.e. spike length) has been kept constant. This curve shows that it is chiefly (iii) which is responsible for raising the graph from a $\frac{1}{|g|^2}$ dependence.

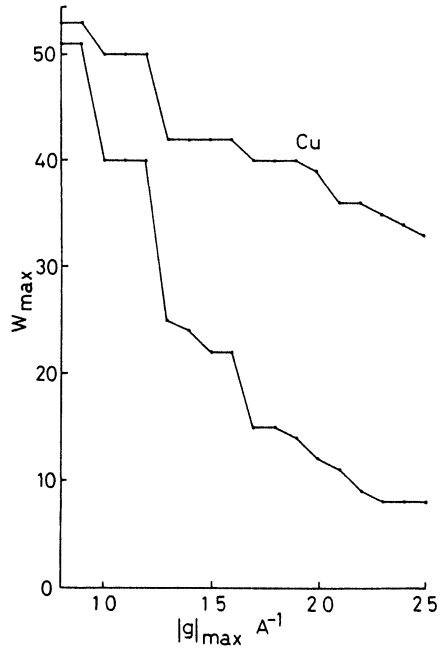

Figure 2. Graphs showing the variation of w_{max} with $|g|_{max}$ for copper and for a material identical to copper, but for which the reciprocal lattice spikes have been artificially adjusted to the same length (i.e. ξ_g is identical for all beams).

The graph seems to predict surprisingly little advantage in using larger g vectors, which is contrary to experience. Two reservations must be made, however:

(a) The calculation does not account for the effects of foil buckling and imperfections in exciting larger g vectors.

(b) w_{max} is largely controlled by orientations located within the area of the unit triangle over which low order zone axis patterns persist without a second zone being excited. Figure 3 shows a unit triangle computed for the case of copper. The hatched areas show the persistence angles before a second zone is excited, for $|g|_{max}$ = 1.5 and 2.0 A^{-1}. It is emphasized that, for example, every location contained within the area surrounding 011 bounded by the $|g|_{max}$ = 1.5 A^{-1} line, will only contain spots from the 011 zone. Increasing $|g|_{max}$ to 2 A^{-1} reduces the proportion of orientation space where this is so, but nevertheless the five nearest appropriately hatched regions closest to 011 will also only contain spots from the 011 zone. Similarly the "neck" nearest the 123 location marks the extent of 123 zone persistence for the appropriate $|g|_{max}$. The remaining locations will contain

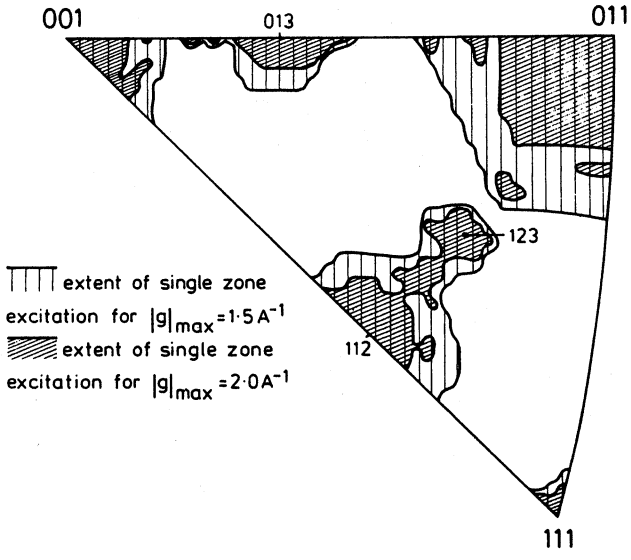

Figure 3. Effect on second zone excitation of increasing the maximum allowed g vector. Orientation determination is more difficult when the crystal is located within the zingle zone excitation region (hatched) for a particular value of $|g|_{max}$ (see text).

only reflections from the 112 zone. (Clearly there must be narrow bands across these necks where both 112 and 123 are present. This is below the 0.5° resolution of the diagram.) Diffraction patterns falling in the hatched regions of Figure 3 in general present more problems than those falling in the clear areas, where more than one zone is present. The particularly difficult areas, mentioned above, where we have to use intensity matching (see Section 4) to analyse the beam directions, are often towards the edges of the hatched areas, where they are crossed by major zones. Orientation determination over the non-difficult areas, while not strictly improved by the increase in $|g|_{max}$, does become very much more convenient.

Evidently, w_{max} as calculated in Figure 2 cannot be interpreted too literally. It is fair to state however that relative changes in w_{max} are still meaningful; as w_{max} rises, for example, the corresponding allowable foil thickness will fall.

Other parameters which influence w_{max} in similar ways to g_{max}, are Debye-Waller factor and lattice paremeter. A large Debye-Waller factor reduces the visibility of the large g vector spots, and raises the w_{max} versus $|g|_{max}$ curve. A large unit cell size reduces all the g vectors, but at the same time the spiking, which depends on the atomic volume, is also reduced. The overall effect of a large unit cell

size is an improvement in orientation resolution.

Crystal structure

The density of points in reciprocal space depends on the size of the primitive cell in real space. For the f.c.c. and b.c.c. structures there is one atom per primitive cell, and the density of points in reciprocal space is dictated by the atomic volume; this determines the lattice parameter, with the effects described above. In the h.c.p. structure there are two atoms in the primitive cell, and the density of points in reciprocal space is twice that expected for an f.c.c. or b.c.c. crystal with the same atomic volume (and species). Figure 4 shows graphs of w_{max} vs $|g|_{max}$ for b.c.c. and h.c.p. "copper" where atomic volume, etc. have been kept constant.

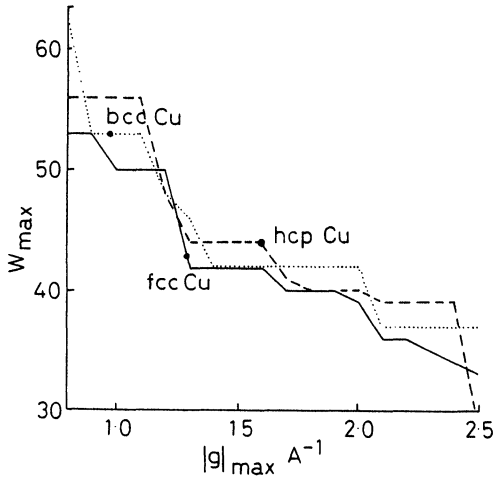

Figure 4. Graphs showing the effect of crystal structure on w_{max} versus $|g|_{max}$ for copper and for h.c.p. and b.c.c. "copper." Atomic volume and Debye-Waller factors are all identical to copper.

The b.c.c. graphs is seen to be almost identical to the f.c.c. one which is also plotted in this figure. The h.c.p. graph is surprisingly similar to f.c.c., given the higher density of points in reciprocal space. Internal interference effects, however, remove a sixth of the points, reduce the spiking of a third of them by a factor of $2/\sqrt{3}$, and that of a further third by a factor of 2.[7] In addition, the ease of orientation determination is more anisotropic for h.c.p. than for f.c.c. crystals. The difficult orientations, as in the case of the f.c.c. system, control the shape of the curves. The angles over which the low index patterns persist before a second zone is visible for a particular $|g|_{max}$ are indicated in Figure 5. Figure 5a shows these boundaries in a standard triangle for the perfect h.c.p. structure for g = 1.5 A^{-1} and 2.0 A^{-1}, and Figure 5b the results for b.c.c. under

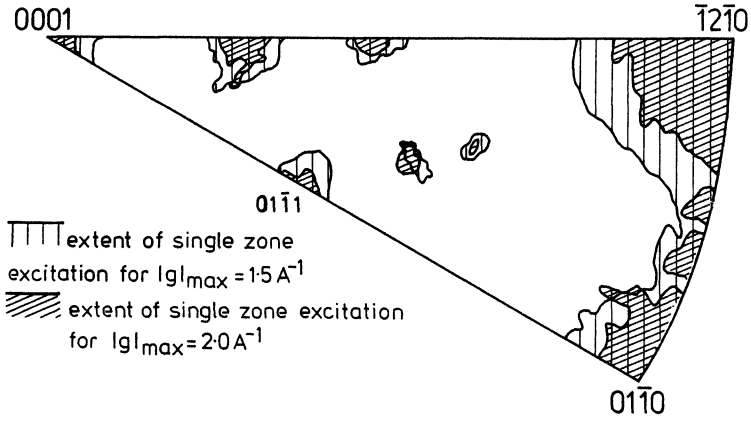

Figure 5a. Effect on second zone excitation of increasing the maximum allowed g vector, for h.c.p. "copper" (identical in all practical respects to the results obtained for titanium).

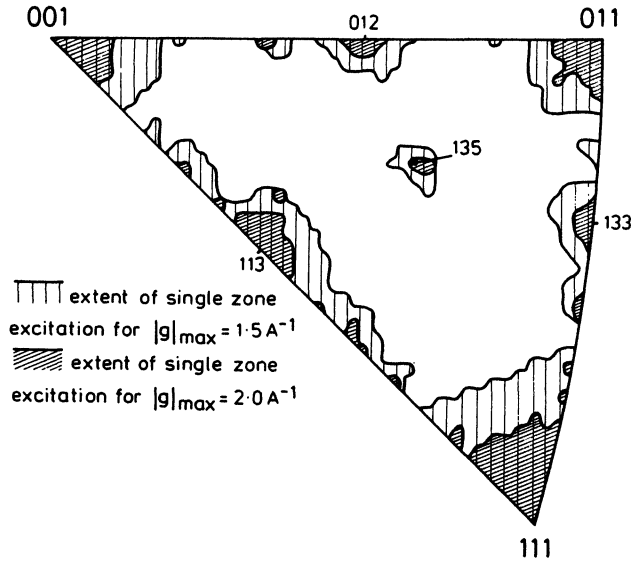

Figure 5b. Effect on second zone excitation of increasing the maximum allowed g vector, for b.c.c. "copper" (identical to iron).

similar conditions.* The hatched areas of the triangles are where the difficult diffraction patterns will be encountered and where care must be exercised in order to prevent artificial orientation clustering.

Orientation determination is evidently very anisotropic for h.c.p., and there is a wide range of difficult orientations associated with the 0002 g vector. The ease of orientation determination over most of the triangle is greater than in the corresponding f.c.c. and b.c.c. cases, although the shape anisotropy of the reciprocal unit cell leads to apparent qualitative similarities between many of the patterns, and additional care must therefore be exercised in the measurements.

Such anisotropy is not inevitable with more complex primitive cells. Thus the more complicated and open a structure, the easier it is to determine its orientation, although there may be orientation regions of exceptional difficulty.

Accelerating voltage

As beam voltage is raised, three factors change (ignoring instrumental features):

(i) The Ewald sphere becomes flatter.
(ii) The extinction distances decrease as 1/v where v is electron velocity.
(iii) The absorption coefficients and diffuse scattering decrease roughly as $1/v^2$.

The effect of (iii) is to raise that value of w_{max} which is acceptable. The effects of (i) and (ii) are demonstrated for copper in Figure 6, which compares the ratios of w_{max} at 1000 kV to that at 100 kV with v_{1000}/v_{100}. The effect of the change in shape of the Ewald sphere is small for $|g|_{max} \simeq 1.7\ A^{-1}$. As $|g|_{max}$ increases the more curved sphere at lower voltages becomes a more efficient sampler of the lattice, since the systematic effect is increasingly removed. Since 1.7 A^{-1} is a typical value for g_{max}, the effect on orientation determination of raising the voltage is to increase the acceptable foil thickness in any particular case in proportion to electron velocity, v, rather than to v^2, as might have been expected.

Figure 7 shows the computed boundaries between single and multiple zone excitations in copper at 100 kV and 1000 kV, for complete cover of the standard triangle with $|g|_{max} = 1.7$. It is clear that the more curved Ewald sphere at 100 kV is only marginally better at exciting second zones under these conditions.

---

*The graphs in Figure 4 and the standard triangles shown in Figure 5 are in all practical respects identical to those computed for titanium (Figure 5a) and for iron (Figure 5b).

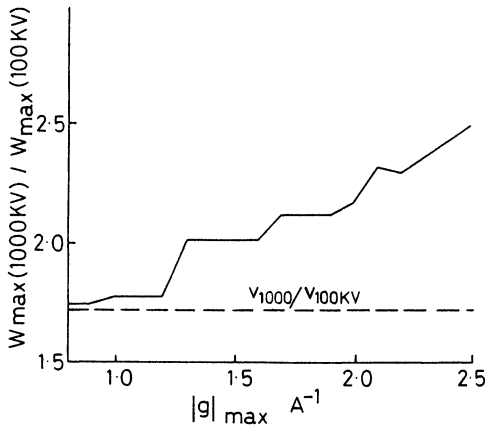

Figure 6. The variation of w_{max}(1000 kV)/w_{max}(100 kV) with $|g|_{max}$. As $|g|_{max}$ decreases, the curvature of the Ewald sphere becomes less important, and w_{max}(1000 kV)/ w_{max}(100 kV) approaches $v_{1000\ kV}/v_{100\ kV}$, the ratio of the electron velocities at the two voltages, which is also the inverse ratio of the reciprocal lattice spiking.

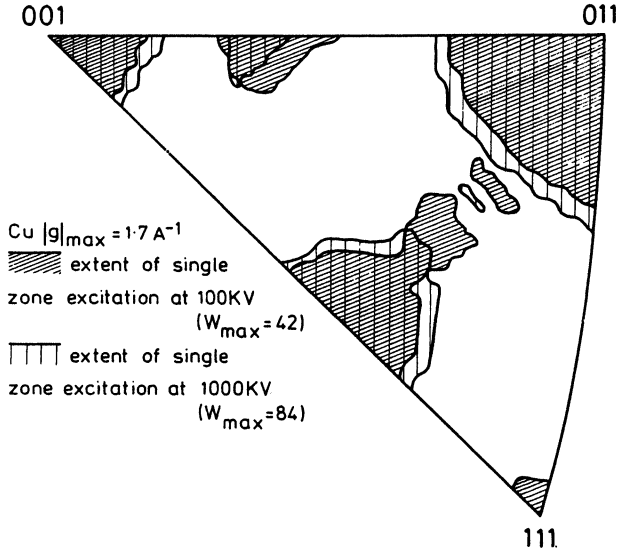

Figure 7. Standard triangle for copper showing the effect of accelerating voltage on the excitation of second zones for $|g|_{max}$ = 1.7 A^{-1}.

4. INTERRELATIONSHIP BETWEEN ORIENTATION DETERMINATION AND AREA SELECTION BY APERTURE

In order to arrive at a minimum crystal diameter necessary to determine orientation, we must measure experimentally the sort of w_{max}, and thus g_{max}, which it is feasible to use, and it is also essential to consider in detail the factors which force us to use larger g vectors than might seem necessary. The worst cases must be considered and these occur, as described in Section 3, in the areas of single zone excitation indicated in Figures 3 and 5, especially towards the edges of these where they are crossed by major zones, when only one systematic row will be strongly excited. Figure 8 shows how the number of mutually non-systematic excited rows

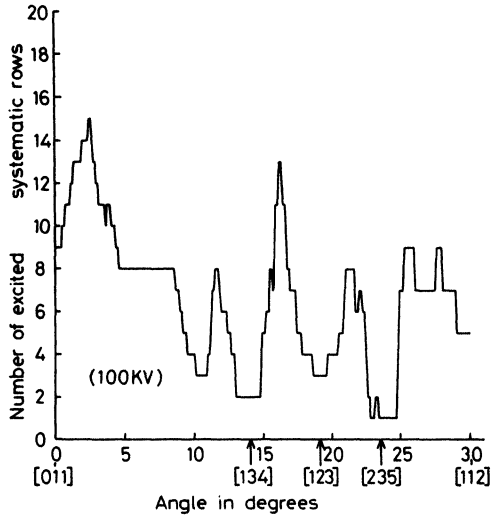

Figure 8. The variation along the 111 Kikuchi band, as it crosses a standard triangle, of the number of excited systematic rows in a copper crystal with a beam voltage of 100 kV. The major poles encountered are indicated below the abscissa. The crystal is set at the symmetry orientation for the 111 row.

of diffraction spots varies with orientation across the standard triangle for a 111 g vector at the symmetry orientation, with a $|g|_{max}$ of 2 A^{-1}.

Consider the diffraction pattern in Figure 9 taken from a relatively flat copper foil which had been tilted a few degrees from <011> towards <123>, in a microscope carefully adjusted so that the projector lens bore directly limited the outermost spots visible. The circles are drawn at $|g|_{max}$ = 1.7 A^{-1} and 2.5 A^{-1}, which correspond to two concentric areas on the foil. Application of the first Ryder-Pitsch method[5] assuming that $4\bar{6}4$ and $11\bar{1}$ lie on the sphere gives a beam direction 13.5° from <011>. Alternatively placing $\bar{3}\bar{5}5$ on the

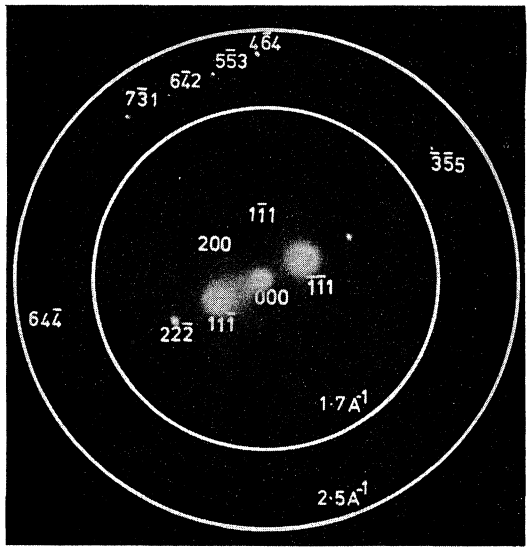

Figure 9. A diffraction pattern from a flat copper foil photographed in an EM300 operating at 100 kV. The crystal is oriented between $|0\bar{1}1|$ and $|123|$ close to the symmetry orientation of the $11\bar{1}$ systematic row. The two scribed circles are for $|g|_{max}$ = 1.7 A^{-1} and 2.5 A^{-1}.

sphere gives a beam direction 13° from <011>, which is within the accuracy claimed for the method.* Two points must be made; the selected spots lay at a radius greater than 1.7 A^{-1} and they were clearly very close to the Ewald sphere. If spots within the circle $|g|_{max}$ = 1.7 A^{-1} are alone considered, then it is clear that the Ryder-Pitsch method is not applicable as there are not two non-systematic spots close to the Ewald sphere.

We have devised a method of matching diffraction patterns in terms of relative intensity for use when Ryder-Pitsch is not applicable. The method assumes that the foil surfaces are roughly parallel, and when this condition is not satisfied it will not work. The technique simply consists of arranging the beams, by inspection, into order of intensity. A preliminary indexing of the beam direction is made and the intensity of each beam calculated according to Equation 4. The beam direction <UVW> is then altered by small amounts until the order of beam intensity calculated agrees with that found by inspection. (It is in fact more convenient to use the expression (- ln w) rather than $1/w^2$ in the calculation.)

For example, in Figure 9 the beams are ordered as follows: $11\bar{1}$, $\bar{1}\bar{1}1$, $22\bar{2}$, $\bar{2}\bar{2}2$, $33\bar{3}$, $\bar{3}\bar{3}3$, $\bar{2}\bar{4}4$. A certain amount

*$11\bar{1}$ was chosen in preference to $\bar{1}\bar{1}1$ because $22\bar{2}$ is slightly brighter than $\bar{2}\bar{2}2$. If however $\bar{1}\bar{1}1$ were chosen the resulting beam direction is 5° closer to 011. This Ryder-Pitsch method[5] is very sensitive when the relevant *g* vectors enclose a small angle.

of common sense must be used. For instance, it is clear on inspecting the $\bar{1}\bar{1}1$, $\bar{2}\bar{2}2$, and $\bar{3}\bar{3}3$ beams that $\bar{4}\bar{4}4$ will be well-nigh, if not actually invisible. $\bar{2}\bar{4}4$ is therefore placed, in terms of intensity, between $\bar{3}\bar{3}3$ and $\bar{4}\bar{4}4$, and much closer to $\bar{4}\bar{4}4$. This comparison of non-systematic with high-order systematic beams is always the crucial step. In this case, such a requirement places the beam direction in a small band centred on [.227, .852, 1.073], which is taken as the final beam direction and is 11½° from [011]. There is a discrepancy of ∿ 2° between this beam direction and that determined by assuming that $4\bar{6}4$ or neighbouring spots lie on the Ewald sphere. This is because these spots arose from a region of the crystal some distance from that giving rise to the more central beams and the disc, although an exceptionally flat copper single crystal, is bent to this extent.

After extensive examination of the difficult areas of orientation space in copper, it has been found possible, using intensity matching, to achieve an accuracy substantially better than 2° anywhere in the unit triangle provided g_{max} is at least 1.7 A^{-1}. This accuracy has been confirmed by comparison with Kikuchi line measurement.

Having arrived at this figure for $|g|_{max}$, which specifies α_{min} for 2° orientation accuracy over the whole triangle, it is possible to evaluate the positional errors using Equation 1. Experiments using gold and aluminium foils in a Philips EM 300 and an AEI EM7 showed that at magnifications of ∿ 20,000-40,000 it was possible to focus to within 3 μm of the specimen at 100 kV and within 10 μm at 1000 kV. The most convenient method, especially at the lower beam voltage, was to image in dark field using a small *g* vector without tilting the beam, and then to make the image as nearly coincident as possible with the bright field image. It was found necessary to add a fine control to the SAD aperture focus on the EM7 to achieve the required accuracy.

The manufacturer's figures for C_s for the EM 300 have been confirmed experimentally, while C_s for the EM7 in side-entry mode has been determined to be 10 mm. This value did not vary with voltage. C_s is expected to be ∿ 6 mm for the same microscope in top entry mode. The relevant data are contained in Table 1.

Figure 10 shows graphs of positional uncertainty ΔR (Equation 1) against $|g|_{max}$ for various operating conditions of an EM 300 and EM7. Evidently ΔR is dominated by spherical aberration at 100 kV and by defocus at 1000 kV. It is clear that the high voltage microscope, particularly in top entry mode, is the preferred technique. The advantages of strong pole pieces are twofold. C_s is nearly halved, and since the objective magnification is raised, the area on the specimen corresponding to the same aperture is reduced. There is clearly little point in trying to reduce ΔR much below d/M, the diameter of the area selected at the specimen. The area localisation can be improved by reducing the aperture diameter

Table 1. Relevant microscope constants for Philips EM 300 and AEI EM7.

Microscope	Pole Piece	Beam Voltage (kV)	Focussing Accuracy μm	Objective Magnification M	C_s mm	g = 1.7 A^{-1}	
						$D\alpha$ Å	$C_s\alpha^3$ Å
EM 300	standard	100	3	10	3.2	1887	7964
	strong	100	3	25	1.7	1887	4231
EM7	side entry	400	7	26	10	838	2183
		1000	10	26	10	445	195
	top entry	1000	10	40	6†		

† estimated (J. Davy, private communication).

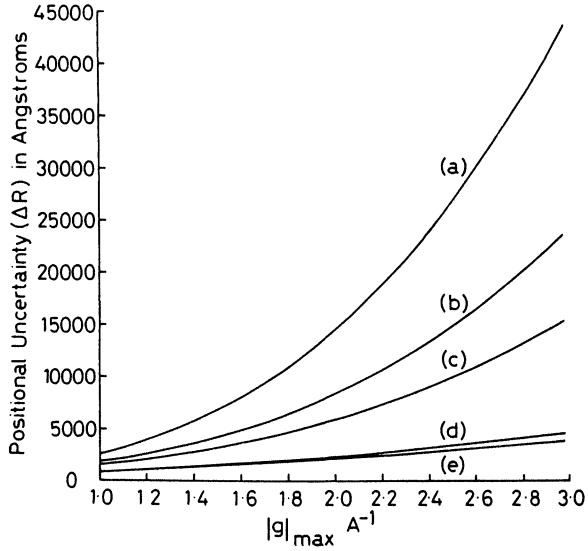

Figure 10. The variation of ΔR ($=C_s\alpha^3 + D\alpha$) with $|g|_{max}$ for an EM300 and EM7 under various operating conditions (see Table 1). (a) EM300, 100 kV, standard pole piece (C_s = 3.2 mm), defocus = 3 μm. (b) EM300, 100 kV, strong pole piece (C_s = 1.7 mm), defocus = 3 μm. (c) EM7, 400 kV, side entry (C_s = 10 mm), defocus = 7 μm. (d) EM7, 1000 kV, side entry (C_s = 10 mm), defocus = 10 μm. (e) EM7, 1000 kV, top entry (C_s = 6 mm), defocus = 10 μm.

but below ∿ 5 μm for foils of average thickness, consistent with good resolution, beam intensity becomes a problem, particularly for microscopes with conventional thermionic guns.

We thus conclude for the case of area selection by aperture that the limit of area selection ($d/M + 2\Delta R$) is ∿ 4000 Å

at 1000 kV in side entry mode, and 14,000 Å for a modern 100 kV microscope with $|g|_{max} = 1.7\ A^{-1}$, and for an aperture size of 5 μm in both cases.

5. DISCUSSION

The main conclusions of Sections 2 and 3 may be summarized as follows:

(i) Given a maximum value of g, g_{max}, there is a maximum value of w, w_{max}, corresponding to the minimum spot intensity it is necessary to accept in order to solve beam directions over the whole standard triangle. In any given set of circumstances (material, foil thickness, beam voltage) this value of w_{max} will correspond to a beam intensity which may or may not be visible.

(ii) Factors which make orientation determination easier are (a) large $|g|_{max}$, (b) high beam voltage, (c) large unit cell, (d) low atomic number, (e) low Debye-Waller factor.

(iii) When the accelerating voltage is raised, the increase in penetration without regard to positional uncertainty is proportional to electron velocity while for constant positional uncertainty it increases more rapidly.

(iv) Crystal structures with lower symmetry may have very anisotropic orientation resolution properties.

(v) Diffraction spot intensity must be taken into account as well as pattern geometry in difficult orientations, where only one systematic row is prominent, in order to prevent artificial clustering of beam directions.

(vi) There is a minimum g_{max} below which the matching or Ryder-Pitsch technique cannot be used everywhere in the standard triangle. This is $\sim 1.7\ A^{-1}$ in copper.

(vii) For area selection by aperture consistent with 2° resolution over the whole standard triangle, positional uncertainty is ~ 1.4 μm at 100 kV and ~ 4000 Å at 1 MV in side entry mode. In thick foils these figures may be considerably increased.

The resolution of the problems posed in this work clearly lie either in HVEM or with STEM[8,9] depending on the importance of electron penetration in the experiment.[10] A report comparing SAD in conventional 100 kV microscopes with HVEM and STEM is being prepared.[11]

It has been demonstrated that beam direction determination in some parts of the stereographic triangle needs *g* vectors of $1.7\ A^{-1}$, while other stereographic locations require shorter vectors in order to give reasonable orientation accuracy. ΔR therefore varies with the stereographic location of the crystal in the unit triangle. The minimum crystal size necessary for a beam direction to be determined also varies in the same way as ΔR, because if a small crystal has a high index beam direction involving large *g* vectors, although the size of the SAD aperture may be increased in order that the whole pattern may appear, the crystal is now a small proportion of the total diffracting volume contributing

to the pattern, and the corresponding high index pattern becomes impossible to distinguish and identify.

In the difficult parts of the unit triangle, ΔR for a fairly typical 100 kV microscope is 1.4 μm, which is large compared with the average subgrain width in sections perpendicular to the sheet plane (e.g. copper $\sim$ 2000 Å[12] and iron $\sim$ 3000 Å[13]).

When deformed metals are studied using SAD with the intention of establishing either texture or neighbour/neighbour orientation relationships, three basic methods are available.

(i) to determine the orientations of as many single crystallites as possible and to relate the measurements to the deformation frame.

(ii) to methodically scan samples using a raster of known pitch. This was developed to allow morphology and orientation to be combined on an orientation topograph.[12]

(iii) to place a large aperture over the area concerned and examine the resultant diffraction pattern for bright reflections which arise from a single zone. A spread about the beam direction in such patterns is common, and it is usually assumed that reflections are bright because several crystallites of similar orientation are contributing to the spots.

In all of these methods the reference frame is determined by noting either an edge cut parallel to one of the primary deformation directions, or in some cases, after severe deformation, the substructure itself is very perfectly aligned with one of the working directions. The beam direction contains information about another reference direction if the specimen is taken from a known section of the worked material.

Method (i) fails because orientation information from crystals of less than 1.4 μm diameter will tend to artificially cluster near low index poles. In copper which has been heavily rolled, for example, comparison of Figure 3 and the raw data of several published investigations reveals some remarkable similarities (e.g. Refs. 12, 14-18). Attempts to correlate the changes in recovered structures with orientation are doubtful for similar reasons,[13,19] and the evidence supporting in-situ nucleation mechanisms, when this is derived from SAD, is clearly open to severe criticism.

The second method may be objected to on the grounds that unless the deformed material is oriented very close to a low index pole then the diffracted beams come from an area encompassing several raster positions simultaneously,[12,20] and for these reasons the accuracy of recently published orientation distribution functions for heavily rolled copper and CuZn[21] which were based on earlier orientation determinations at 100 kV[15,16,18] cannot be as high as the authors claim.

There are two objections to method (iii), the most obvious being artificial orientation clustering near to low index zones due to the small crystallite size. In addition, there are problems caused by diffracted beam "size." Any crystallites oriented close to a low index zone will contribute to the resulting diffraction pattern. This will be so even when the crystallites are rotated away from the low order beam direction, because of the large reciprocal lattice spiking of low order reflections. Thus a large volume of material

can contribute significant intensity in the diffraction pattern if it is located within 15° of low index poles. On the other hand, if this same volume of material is distributed in the same way about a high index beam direction, only very similarly oriented crystallites will produce bright diffracted beams because reciprocal lattice spiking associated with high index diffracted beams is small (see Section 3). Thus orientation clustering which occurs near low index zones will not be reproduced near high index zones. Clearly rotations around the beam direction in the plane of the diffraction pattern can be accurately assessed.

In conclusion, a large part of the experimental work on textures using SAD in conventional electron microscopes is suspect, and should be repeated using either STEM or HVEM.

ACKNOWLEDGEMENTS

Financial support for this work was provided by the S.R.C. through grant B/RG/6843.2 (BJD) and in the form of a research fellowship (IPJ). The authors are grateful to Professor R. E. Smallman for the provision of laboratory facilities and for his interest in the work. They also acknowledge many helpful discussions with their colleagues, especially Drs. M. H. Loretto and W. B. Hutchinson, and Professor M. Hatherly.

REFERENCES

1. W. Pitsch, H. J. Perlwitz and K. Lücke, *Zeit. für Metall.*, 61, 232 (1970).
2. B. J. Duggan and R. L. Segall, *Acta Met.*, 19, 317 (1971).
3. M. Heimendahl, *Prakt. Metall.*, 8, 279 (1971).
4. C. Laird, E. Eichen and W. R. Bitler, *J. Appl. Phys.*, 37, 2225 (1966).
5. P. L. Ryder and W. Pitsch, *Phil. Mag.*, 15, 437 (1967).
6. P. L. Ryder and W. Pitsch, *Phil. Mag.*, 18, 807 (1968).
7. I. P. Jones and E. G. Tapetado, in *Proc. 3rd Int. Conf. on High Voltage Electron Microscopy*, Academic Press, New York, 1974, p. 48.
8. R. Geiss, *Developments in Electron Microscopy and Analysis*, J. Venables, ed., Academic Press, New York, 1976, p. 61.
9. A. G. Craven, *V.G. Microscopes Bulletin*, 1, 2 (1976).
10. D. C. Joy, *Advances in Analyses of Microstructural Features*, Metals Society, London, 1972, p. 20.
11. R. Hutchings, B. J. Duggan and R. E. Smallman, to be published.
12. R. Gotthardt, G. Hoschek, O. Reimold and F. Haessner, *Texture*, 1, 99 (1973).
13. R. L. Every and M. Hatherly, *Texture*, 1, 183 (1974).
14. F. Haessner, U. Jacobowski and M. Wilkens, *Phys. Status Solidi*, 7, 701 (1964).
15. K. Lücke, H. J. Perlwitz and W. Pitsch, *Phys. Status Solidi*, 7, 733 (1964).
16. H. J. Perlwitz, W. Pitsch and K. Lücke, in *Recrystallization, Grain Growth and Textures*, ASM, Metals Park,

Ohio, 1966, p. 367.
17. F. Haessner, *ibid.*, p. 386.
18. H. J. Perlwitz, K. Lücke and W. Pitsch, *Acta Met.*, 17, 1183 (1969).
19. I. L. Dillamore, C. J. E. Smith and T. W. Watson, *Met. Sci. J.*, 1, 49 (1967).
20. F. Haessner, U. Jacobowski and M. Wilkens, *Acta Met.*, 14, 454 (1966).
21. J. Pospiech and K. Lücke, *Acta Met.*, 23, 997 (1975).